

Growth of single-walled carbon nanotubes with controlled diameters and lengths by an aerosol method

Ying Tian, Marina Y. Timmermans, Matti Partanen, Albert G. Nasibulin*, Hua Jiang, Zhen Zhu, Esko I. Kauppinen

NanoMaterials Group, Department of Applied Physics, Center for New Materials, Aalto University, Puumiehenkuja 2, 00076 Aalto, Finland

ARTICLE INFO

Article history:

Received 19 April 2011

Accepted 2 June 2011

Available online 15 June 2011

ABSTRACT

On the basis of combined study of the transmission electron microscopy, scanning electron microscopy, Raman spectroscopy and ultraviolet-visible-near infrared absorption spectroscopy, the properties of the single-walled carbon nanotubes (SWCNTs), synthesized by aerosol (floating catalyst) chemical vapor deposition method by ferrocene vapor decomposition in the presence of carbon monoxide, are studied in details. The results show that increasing the temperature gives rise to the formation of high quality and large diameter SWCNTs. By monitoring the water-cooled probe position, both the bundle length and the diameter of the SWCNTs are effectively tuned due to the variation of the residence time and temperature profile in the reactor. An introduction of a small amount of CO₂ suppresses the growth of small diameter nanotubes and enlarges the mean diameter of SWCNT samples. The mean diameter of SWCNTs could be easily altered in a broad range from 1.1 to 1.9 nm during growth, which is essential for the SWCNT applications in optical and electronic devices.

© 2011 Elsevier Ltd. All rights reserved.

1. Introduction

Due to their unique one-dimensional nanostructure, single-walled carbon nanotubes (SWCNTs) exhibit remarkable mechanical, optical and electrical properties making them suitable for a wide range of applications such as micro-electromechanical devices [1], sensors [2,3], transparent metal electrodes [4], field-effect transistors [5] and capacitors [6]. Although single-channel devices with individual SWCNTs have been extensively explored, bulk SWCNT materials are more promising for the future application due to their ease in handling, large application area and cost efficiencies [7]. It is known that the chiral angle and diameter of SWCNTs can fully determine their electronic structure. Therefore, the control of diameter is very important for the investigation of physical and electronic properties of nanotubes, and further steering their optical and electronic applications.

Although various techniques have been developed to produce bulk SWCNTs, very few methods can efficiently alter the diameters of the products in a wide range. Usually, each method is suitable for the growth of SWCNTs with certain diameters. For instance, an arc discharge method allows producing SWCNTs with diameters from 1.0 to 1.4 nm by selecting metal catalyst and chamber pressure [8–10]. A laser ablation technique controls the diameter of SWCNTs from 1.0 to 1.3 nm by varying the furnace temperature from 780 to 1200 °C [11]. HiPco (high-pressure CO) method usually produce the SWCNTs with mean diameters about 1.0 nm [12–15]. Additionally, the reported effect of the experimental conditions on the parameters of produced SWCNTs is not always similar for different synthesis methods. Usually, the diameter of SWCNTs increases with the growth temperature [16–19], which is explained by the enlargement of the catalyst particles and their direct correlation with SWCNT diameters [20]

* Corresponding author. Fax: +358 9 2451 3517.

E-mail addresses: albert.nasibulin@aalto.fi, albert.nasibulin@hut.fi (A.G. Nasibulin).

0008-6223/\$ - see front matter © 2011 Elsevier Ltd. All rights reserved.

doi:10.1016/j.carbon.2011.06.036

or by the formation of larger fullerene caps – nuclei for the SWCNTs [19]. Another explanation is that the smaller diameter tubes are less resistant at higher temperatures especially at gently oxidative conditions [15,21]. Nevertheless, some researchers revealed the opposite temperature effect on the CNT diameters [22–24]. Therefore the control and tailoring the diameters of SWCNTs is still an open issue.

Here, for the first time we demonstrate that the mean diameter of SWCNTs can be easily controlled in a broad range from 1.1 to 1.9 nm by altering the synthesis conditions in the same reactor. The experiments were carried out in an aerosol chemical vapor deposition (CVD) reactor based on ferrocene vapor decomposition in an atmosphere of CO [25]. This wide range control of SWCNT diameters gives possibility to adjust the properties of SWCNTs to meet the needs for specific applications. For instance, the absorption peaks of SWCNTs covering the wide range from 500 to 2700 nm allows the fabrication of saturable absorbers, operating in a full range from visible to NIR for ultrafast lasers [26]. Diameter modulation of SWCNTs provides the opportunity for improving the properties of microelectronics by engineering the band gap of semiconducting tubes [27]. Our synthesis method is attractive from commercial point of view, since it allows manufacturing

SWCNT films with adjustable electrical and optical characteristics without detrimental liquid dispersion and purification. The films can be prepared by a simple dry transfer technique from a filter, on which they are collected from the gas phase, to practically any other substrate [28,29]. A detailed investigation of SWCNT products and related growth mechanism is reported as a function of the synthesis reactor temperature, water-cooled probe position and addition of a small amount of CO₂ during growth on the basis of combined analyses of transmission electron microscopy (TEM), scanning electron microscopy (SEM), Raman and ultraviolet–visible–near infrared (UV–Vis–NIR) absorption spectroscopy.

2. Experimental

The growth of SWCNTs, using an aerosol CVD reactor, was described elsewhere [30]. Briefly, carbon monoxide (CO) was used as the carbon source, and ferrocene as the catalyst precursor was vaporized by passing ambient temperature CO with a flow rate of 300 cm³/min through a cartridge filled with the mixed powder of ferrocene and silicon dioxide (weight ratio FeCp₂:SiO₂ = 1:4). The flow containing ferrocene vapor and CO was then introduced directly into the high temperature

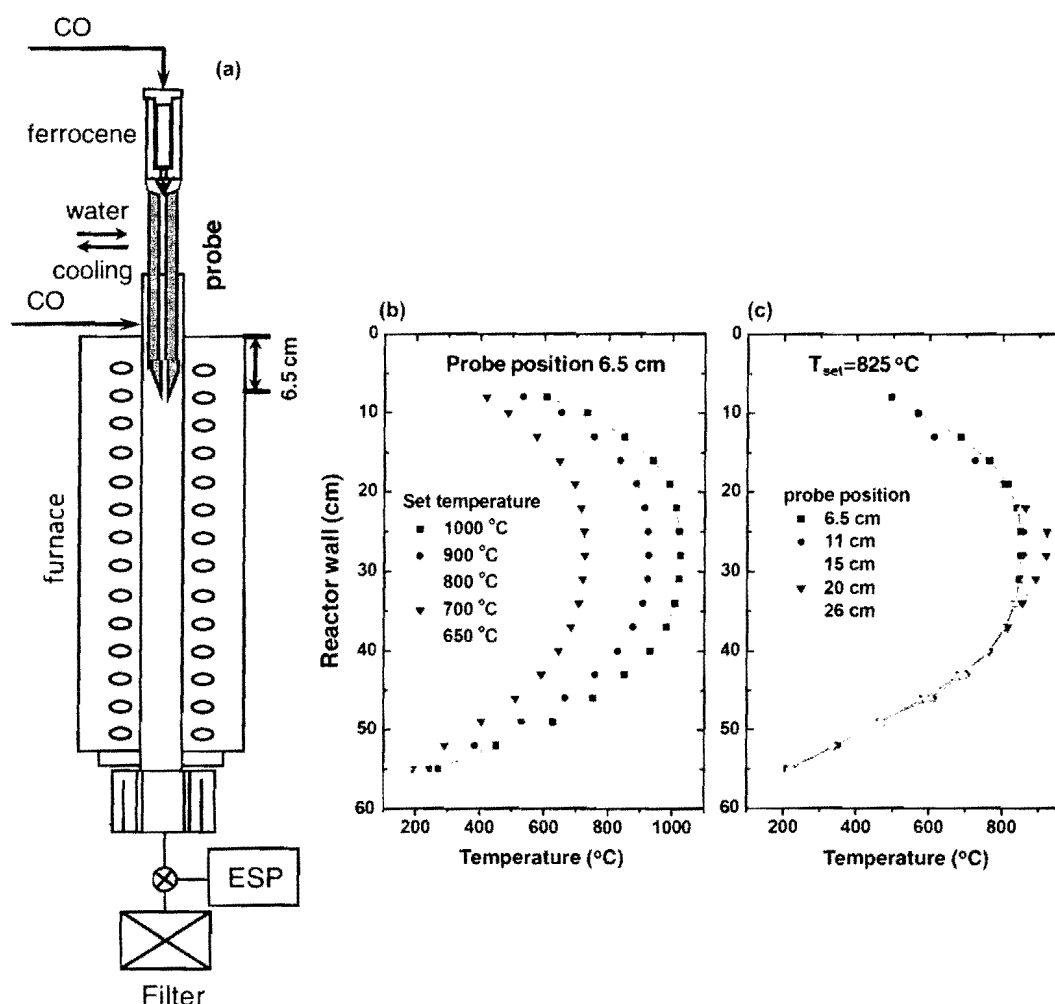


Fig. 1 – (a) Schematic representation of the experimental setup along with the temperature profiles, (b) at water-cooled probe position of 6.5 cm as a function of T_{set} and (c) at $T_{set} = 825$ °C as a function of water-cooled probe position.

zone of the furnace by a water-cooled probe maintained at 24 °C. In order to control the precursor vapor heating rate and residence time, the injector probe position was varied from 6.5 to 29 cm deep in the reactor with a heating zone of 49 cm. The experimental setup is shown in Fig. 1a. Additional CO flow of 100 cm³/min was introduced from outside the water-cooled probe. The temperature profiles were measured by positioning a K-type thermocouple (SAB Bröckskes GmbH and Co., KG, Germany) at various locations in the reactor. The set temperature of the reactor furnace (T_{set}) was varied from 650 to 1000 °C. The maximum wall temperature in the reactor (T_{max}) depended on the probe position, e.g., at 6.5 cm the maximum temperature was 25 °C higher than the set temperature (Fig. 1b and c).

The SWNT samples were collected from the gas phase on TEM grids or by filtering the flow through 2.45 cm diameter nitrocellulose disk filters downstream of the reactor. The as-deposited samples were analyzed using transmission electron microscope (TEM, Philips CM200 FEG), Raman spectrometer (Wintech alpha300) equipped with a Nd:YAG laser at 532 nm (2.33 eV), UV-Vis-NIR absorption spectrometer (Perkin-Elmer Lambda 950) and photoluminescence spectrometer (NSI NanoSpectralyzer). To measure the absorption spectra, the SWCNT sample was deposited by the dry transfer technique from the filter to an optically transparent substrate [28], 1 mm thick quartz window (material: HQS300, Heraeus). An uncoated quartz substrate was used in the reference beam to exclude the effect of the substrate. The bundle length at different probe positions was estimated statistically from SEM images of thin SWCNT networks.

3. Results and discussions

Fig. 2 shows typical TEM images of the as-synthesized SWCNT samples collected at set temperatures of 850, 900, 950 and 1000 °C and at the probe position of 6.5 cm. The products consist of SWCNT bundles along with some individual SWCNTs as can be seen from the inset high-resolution TEM (HRTEM) image. The catalyst particles and a small amount of impurities are observed on the surface of the SWCNTs. The SWCNT bundle length depends on the set temperature of the synthesis reactor. Increasing the temperature resulted in the reduction of the tube length. The purity as well as the diameter distribution of the SWCNTs was also found to be very dependent on the growth temperature, which will be further analyzed by the optical measurements.

Fig. 3a and b show the Raman spectra of the SWCNT samples, synthesized at set temperatures in the range between 850 and 1000 °C, in the radial breathing mode (RBM) as well as G and D band regions, respectively. The RBM features, corresponding to the coherent vibration of the carbon atoms in the radial direction, are signatures of the nanotube diameter through its frequency (ω_{RBM}) defined by the well established equation of $d_t = A/\omega_{\text{RBM}} + B$, where $A = 217.8$ and $B = 15.7$. The RBM spectra excited by 2.33 eV photons in Fig. 3a show similar RBM positions in the region of 130–230 cm⁻¹. However, the central position of the most prominent RBMs shifts to higher frequency direction with the decrease of growth temperature. This indicates that the relative abundance of smaller diameter SWCNTs increases with the decrease of temperature.

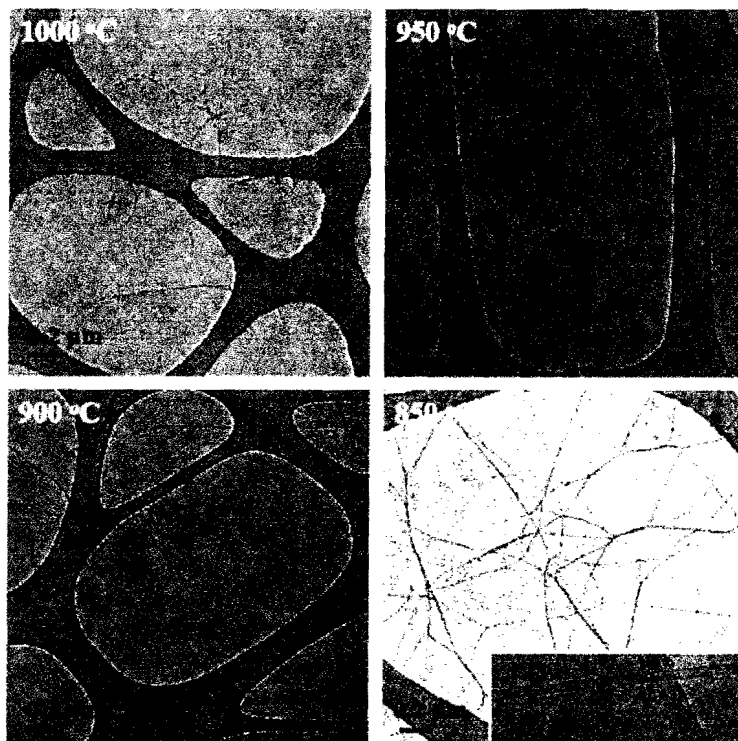


Fig. 2 – TEM images of the SWCNT samples synthesized at a probe position of 6.5 cm as a function of T_{set} . The inset shows a high-resolution TEM image.

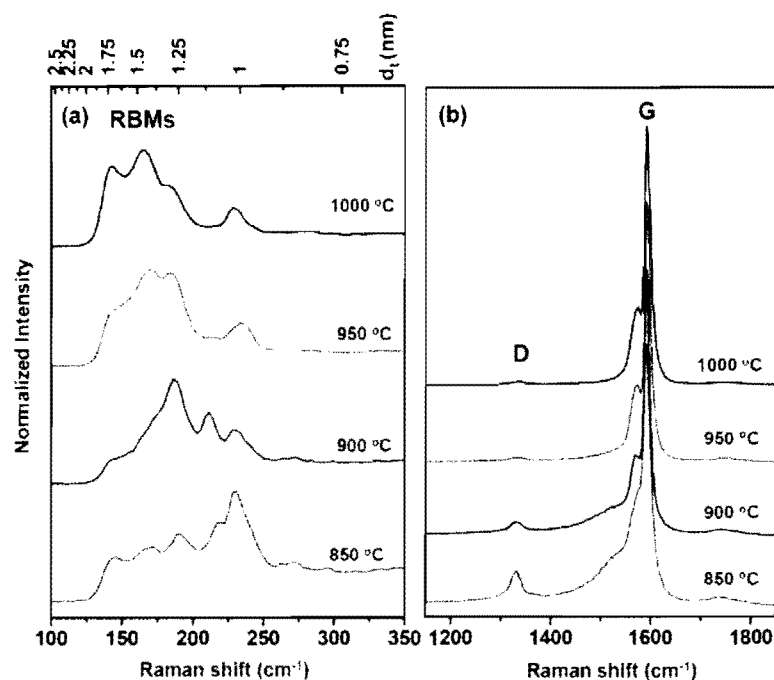


Fig. 3 – Raman spectra in the regions of (a) RBMs and (b) G and D bands of the SWCNT samples collected at a probe position of 6.5 cm as a function of T_{set} . The RBM spectra excited by 2.33 eV photons.

The G band involves the vibration of sp^2 -bonded carbon atoms in the graphite layer, while the D band is related to the disorder-induced mode in SWCNTs. The Raman spectra in the region of G and D modes are normalized to the height of G peaks. It is clearly shown that the intensity of D band decreases with increasing the temperature. This is understandable since defects are annealed away at higher temperature, which results in the more crystalline graphitic nanotube walls [31].

Raman spectroscopy allows detecting only SWCNTs that are in resonance with the excitation energy. Therefore UV–Vis–NIR absorption spectrometer was further applied to characterize the full diameter distribution of the SWCNT samples. Fig. 4a shows that the absorption spectra of the SWCNT samples collected at different set temperature from 850 to 1000 °C at water-cooled probe position of 6.5 cm. The absorption peaks from the first electronic transition of the semiconducting nanotube (E_{11}^S) present clearly the bimodal shape in the range of 1500–2500 nm for the samples synthesized at 1000 and 950 °C. Decreasing the temperature to 900 °C, the absorption peaks exhibit mono-modal distribution with narrower peak width and the peak positions shift to the shorter wavelength (higher energy). This implies the decrease of the nanotube diameter along with a narrower diameter distribution. The absorption peaks continuously shift to higher energy for the sample produced at 850 °C, which indicates the smaller diameter of SWCNTs collected at lower temperature. This result is consistent with the Raman analysis (Fig. 3a). To quantify the diameter distribution of SWCNTs based on the optical absorption spectra, we model the optical absorption as linear composition of each nanotube type. The transition energies of a SWNT are described by a sum of Gaussian line shapes describing the broadening of each optical transition due to

the finite lifetime and finite resolution of the spectrometer. The highly ill-posed problem is well resolved by the introduction of a regularization term in the fitting process [32]. By using this method, the fitted diameter diagrams are shown in Fig. 4b. The mean diameter of the SWCNT samples increases from 1.2 to 1.7 nm with the temperature. For the samples collected at 1000 and 950 °C, there are about 80% nanotubes with a diameter in the range of 1.2–2.0 nm. However, the most abundant diameter fractions are in the range of 1.6–2.0 and 1.2–1.6 nm for the sample at 1000 and 950 °C, respectively. For the SWCNT sample synthesized at 900 °C, the diameter diagram presents narrower diameter distribution of 1.3 ± 0.2 nm. Interestingly, although the mean diameter continuously decreases at the temperature of 850 °C and about 70% nanotubes are in the range of 0.8–1.4 nm in diameter, there is a small tail left in the higher diameter range from 1.6 to 2.0 nm. The photoluminescence emission/excitation (PLE) spectra (Fig. 5) again confirm the diameter variation with the growth temperature. At 900 °C, the PLE map shows most abundant semiconducting nanotubes at the emission ranges of 1300–1400 and 1500–1600 nm; while at higher temperature of 1000 °C, the diameter of SWCNT sample becomes larger and only few of SWCNTs are within the detection range of the PLE spectroscopy shown as the weak bright spots in Fig. 5b. This again confirms the low yield of the small diameter nanotubes in SWCNT sample grown at high temperatures.

It has been previously observed that the temperature increase results in an increase in the catalyst particle size due to the higher rate of agglomeration of primary particles, which results in the formation of larger diameter nanotubes due to the directly proportional relationship between catalyst particle size and diameter of nanotubes [33,34]. The results analyzed by Raman, absorption and PLE spectra in this work

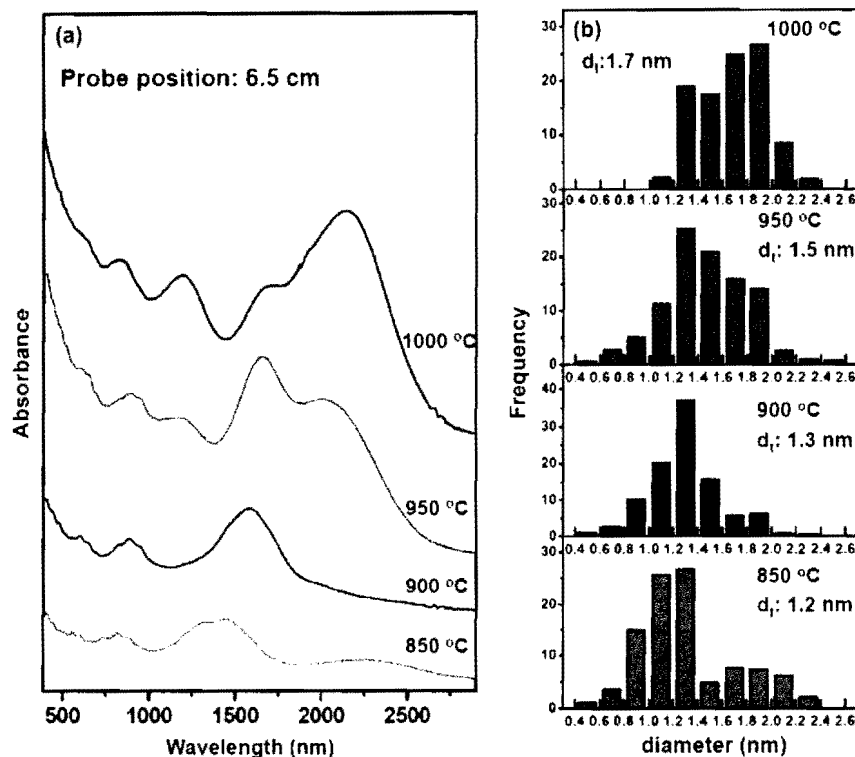


Fig. 4 – (a) UV-Vis-NIR absorption spectra and (b) the correspondence fitted diameter diagrams of the SWCNT samples collected as a function of T_{set} at a probe position of 6.5 cm. The mean diameters (d_i) increase from 1.2 to 1.7 nm along with the temperature.

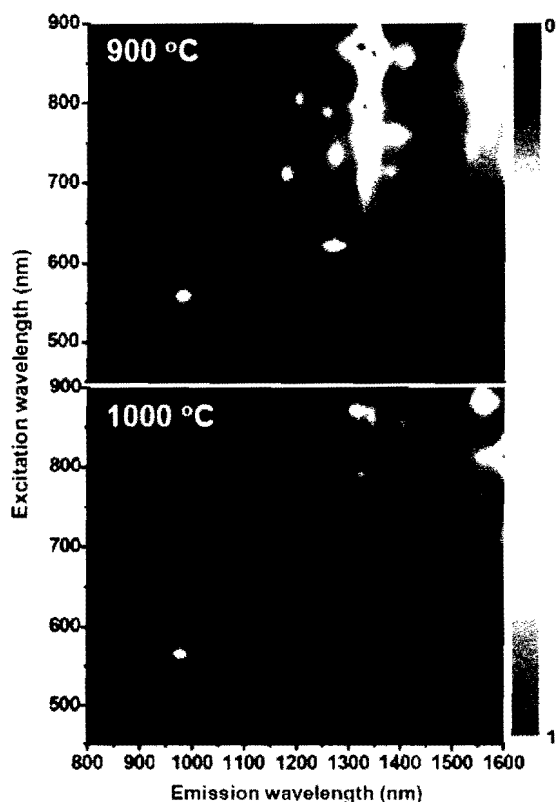


Fig. 5 – Contour plots of photoluminescence spectra of the SWCNT samples collected at $T_{\text{set}} = 900$ and 1000 °C at probe position of 6.5 cm.

support the above observation. Additionally, the bimodal diameter distribution of the SWCNTs shown in the absorption spectra may correlate to the bimodal size distribution of catalyst particles. This aspect suggests the importance of further studies on this topic.

When the water-cooled probe is inserted deeper into the reactor down to 15 cm, it allows us to grow the SWCNTs at as low as 650 °C (reactor set temperature). The absorption spectra of the SWCNT samples grown at T_{set} from 650 to 1000 °C are shown in Fig. 6a. Using the same fitting method, the derived mean diameter of the SWCNT sample increases from 1.1 to 1.7 nm with the temperature increase (Fig. 6b). To study the effects of the water-cooled probe position on the properties of SWCNT products, the absorption spectra of the SWCNT samples collected as a function of probe positions at set temperature of 825 °C are shown in Fig. 7a. Interestingly, the diameter of the SWCNTs first increases from 1.2 to 1.6 nm with the probe position continuously lowered from 6.5 to 23 cm (measured from the inlet of the furnace, experimental setup in Fig. 1). At the position deeper than 23 cm the mean diameter of the SWCNTs starts to decrease to 1.2 nm (at the probe position of 29 cm). The water-cooled probe position influences both the temperature profile and the residence time in the reactor.

The temperature profiles shown in Fig. 1a indicate that the maximum wall temperature of the reactor is about 25 °C higher than the set temperature at probe position of 6.5 cm. The maximum temperature zone is about 10 cm long around the middle of the furnace. Fig. 1b shows that the temperature profiles vary as a function of the probe position at the same set

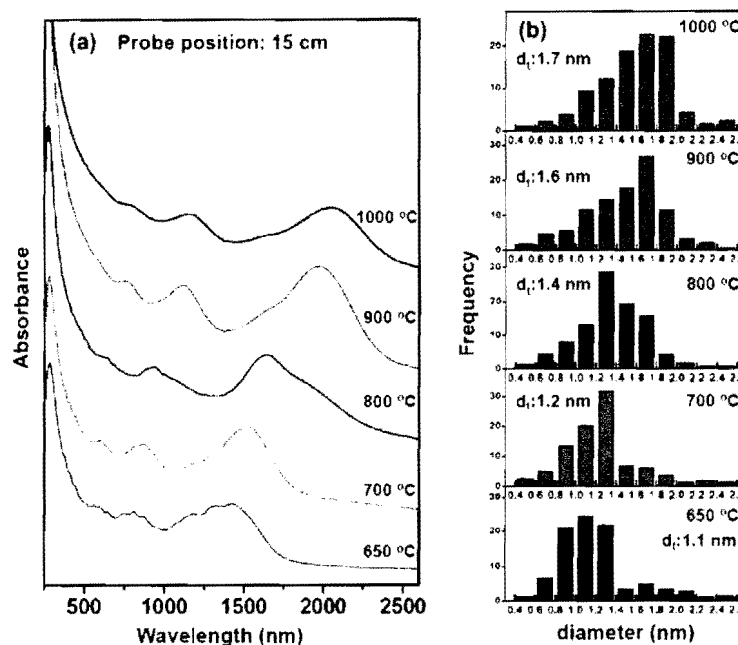


Fig. 6 – (a) UV-Vis-NIR absorption spectra and (b) the corresponding fitted diameter diagrams of the SWCNT samples collected at probe position of 15 cm as function of T_{set} . The mean diameters of SWCNTs collected at $T_{\text{set}} = 650, 700, 800, 900, 1000$ °C are 1.1, 1.2, 1.4, 1.6, 1.7 nm, respectively.

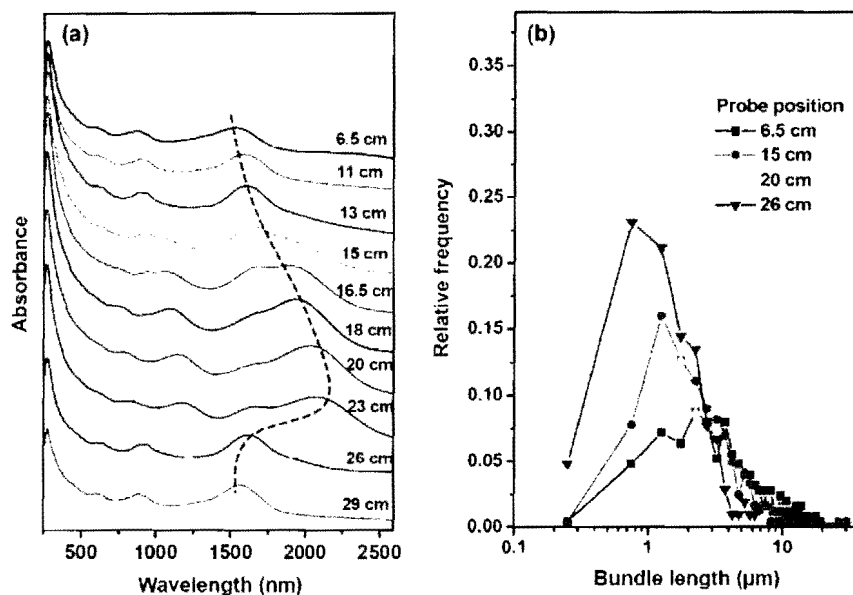


Fig. 7 – (a) UV-Vis-NIR absorption spectra and (b) bundle length distributions of the SWCNT samples synthesized at $T_{\text{set}} = 825$ °C as function of water-cooled probe position.

temperature of 825 °C. The maximum wall temperature of the reactor increases from 850 to 920 °C with the position of the water-cooled probe moved from 6.5 to 20 cm. While the probe position is deeper than 26 cm, the maximum temperature of the reactor starts to decrease. The reason can be explained due to the fact that the reactor is a two heating zone reactor, which is controlled by two thermocouples located at 21 and 36 cm, respectively. The deeper the probe position, the higher the cooling and, as a result the heating elements of the furnace work with higher power to keep the set temperature of

825 °C at 21 cm. This results in higher maximum wall temperature in the middle of the furnace. Thus the maximum wall temperature increases with the probe position. However, when the probe position exceeded the middle of the furnace (deeper than 26 cm), the whole upper part of the heating zone is cooled down by the probe, which makes lower maximum wall temperature of the reactor. As shown in Fig. 1b, the maximum wall temperature of the reactor is 815 °C at probe position of 26 cm ($T_{\text{set}} = 825$ °C). These temperature profiles explain the results of the absorption measurements in

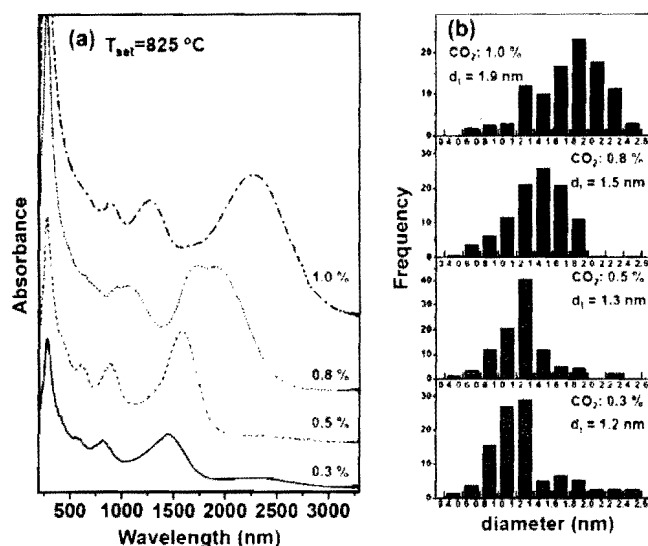


Fig. 8 – (a) UV-Vis-NIR absorption spectra and (b) the fitted diameter diagrams of the SWCNT samples collected at $T_{\text{set}} = 825\text{ }^{\circ}\text{C}$ at probe position of 6.5 cm as function of CO_2 concentration.

Fig. 7a, i.e. the mean diameter of SWCNTs increases first with the probe position and then decreases after the probe position is deeper than 23 cm.

In addition, the bundle length of the SWCNTs also depends on the probe position as shown in Fig. 7b. The length of SWCNTs first decreases with the probe position and then increases at the probe position of 26 cm. It is believed that the length of SWCNT can be controlled by both the residence time and the temperature. On the basis of in situ sampling experiments, it was found that the growth of SWCNT stops when the temperature is higher than $928\text{ }^{\circ}\text{C}$ due to the thermodynamic restriction of the CO-disproportionation reaction at high temperatures [25]. Similar experimental phenomenon was also observed in another aerosol system (hot wire generator reactor), where the growth of SWCNTs stops at a temperature of $908\text{ }^{\circ}\text{C}$ [35]. When the temperature is below $900\text{ }^{\circ}\text{C}$, the SWCNTs continuously grow throughout the reactor, staying longer in the high temperature zone. This also explains the observation of TEM images in Fig. 2 that the bundle length increases with the decrease of temperature. In the case of $T_{\text{max}} = 900\text{ }^{\circ}\text{C}$, the residence time in the reactor plays an important role on the length of SWCNTs. As shown in Fig. 7b, the average bundle lengths of SWCNTs collected at the probe position of 6.5, 15, 26 cm are 5.4 ± 4.1 , 3.6 ± 3.5 , $1.8 \pm 1.2\text{ }\mu\text{m}$, respectively. However, for the SWCNT sample synthesized at the probe position of 20 cm, the bundle length is the shortest of about $1.2 \pm 0.8\text{ }\mu\text{m}$ due to the high maximum wall temperature about $920\text{ }^{\circ}\text{C}$ of the reactor. Therefore, by simply moving the probe position, the residence time and temperature profile of the reactor changes efficiently. This provides a possibility of altering the mean diameter, diameter distribution and the length of SWCNT products. Here, it is important to note that the length of individual tubes is not necessarily linearly proportional to the bundle length. However, since the bundle diameter does not vary significantly

[28], generally we can state that the lengths of the bundles and individual tubes correlate.

Also it has been found that CO_2 plays an essential role in the SWCNT growth [36]. The absorption spectra of the SWCNT samples collected at $T_{\text{set}} = 825\text{ }^{\circ}\text{C}$ with different CO_2 concentrations are shown in the Fig. 8a. It can be observed that the absorption peaks significantly shift to longer wavelength with the increase of CO_2 concentration. This indicates that the diameter of SWCNTs increases with the CO_2 concentration. Using the same fitting program, the derived mean diameters of the SWCNTs are 1.2, 1.3, 1.5 and 1.9 nm for the CO_2 concentration of 0.3%, 0.6%, 0.8%, and 1.0%, respectively (Fig. 8b). The nucleation of CNTs is believed to occur from solid iron supersaturated by carbon. Carbon released on the surface forms a graphitic cap (a CNT nucleation site). When CO_2 as an etching agent is present in the system, it can selectively etch the more reactive carbon atoms in the graphitic cap of high curvature due to the inverse Boudouard reaction. As a result, the growth of small diameter nanotubes is suppressed and the mean diameter of SWCNT products is enlarged with the CO_2 concentration as observed in Fig. 8.

4. Conclusions

We have synthesized SWCNTs in an aerosol CVD reactor using CO as the carbon source and ferrocene as the catalyst precursor. By changing the growth conditions, the mean diameter of SWCNTs can be effectively tailored in a broad range from 1.1 to 1.9 nm. Increasing temperature results in the formation of high quality and larger diameter SWCNTs. We have found that the water-cooled probe position can tune both the length and diameter of SWCNTs by varying the residence time and temperature profile of the reactor at the same time. The length dependence on the probe position supports the fact that the nanotube growth stops at the temperature higher than $900\text{ }^{\circ}\text{C}$. The effects of CO_2 on the diameter of SWCNTs are also studied. The selective etching of small diameter nanotubes by CO_2 provides a way of controlling the mean diameter and diameter distribution of the SWCNT products.

Acknowledgements

This work was supported by the Academy of Finland (project numbers 128445 and 128495) and Aalto University through the Multidisciplinary Institute of Digitalization and Energy (CNB-E project) program.

REFERENCES

- [1] Hayamizu Y, Yamada T, Mizuno K, Davis RC, Futaba DN, Yumura M, et al. Integrated three-dimensional microelectromechanical devices from processable carbon nanotube wafers. *Nat Nano* 2008;3(5):289–94.
- [2] Kong J, Franklin NR, Zhou C, Chapline MG, Peng S, Cho K, et al. Nanotube molecular wires as chemical sensors. *Science* 2000;287(5453):622–5.

- [3] Collins PG, Bradley K, Ishigami M, Zettl A. Extreme oxygen sensitivity of electronic properties of carbon nanotubes. *Science* 2000;287(5459):1801–4.
- [4] Zhang D, Ryu K, Liu X, Polikarpov E, Ly J, Tompson ME, et al. Transparent, conductive, and flexible carbon nanotube films and their application in organic light-emitting diodes. *Nano Lett* 2006;6(9):1880–6.
- [5] Artukovic E, Kaempgen M, Hecht DS, Roth S, Grüner G. Transparent and flexible carbon nanotube transistors. *Nano Lett* 2005;5(4):757–60.
- [6] Futaba DN, Hata K, Yamada T, Hiraoka T, Hayamizu Y, Kakudate Y, et al. Shape-engineerable and highly densely packed single-walled carbon nanotubes and their application as super-capacitor electrodes. *Nat Mater* 2006;5(12):987–94.
- [7] Duong HM, Ishikawa K, Okawa J, Ogura K, Einarsson E, Shiomi J, et al. Mechanism and optimization of metal deposition onto vertically aligned single-walled carbon nanotube arrays. *J Phys Chem* 2009;C113(32):14230–5.
- [8] Shi Z, Lian Y, Zhou X, Gu Z, Zhang Y, Iijima S, et al. Mass-production of single-wall carbon nanotubes by arc discharge method. *Carbon* 1999;37(9):1449–53.
- [9] Saito Y, Tani Y, Kasuya A. Diameters of single-wall carbon nanotubes depending on helium gas pressure in an arc discharge. *J Phys Chem* 2000;B104(11):2495–9.
- [10] Kasuya A, Sasaki Y, Saito Y, Tohji K, Nishina Y. Evidence for size-dependent discrete dispersions in single-wall nanotubes. *Phys Rev Lett* 1997;78(23):4434–7.
- [11] Bandow S, Asaka S, Saito Y, Rao AM, Grigorian L, Richter E, et al. Effect of the growth temperature on the diameter distribution and chirality of single-wall carbon nanotubes. *Phys Rev Lett* 1998;80(17):3779–82.
- [12] Rosario-Castroa BI, Contesa EJ, Lebrón-Colón M, Meadorc MA, Sánchez-Pomalesa G, Cabrera CR. Combined electron microscopy and spectroscopy characterization of as-received acid purified and oxidized HiPCO single-wall carbon nanotubes. *Mater Charact* 2009;60(12):1442–53.
- [13] Kukovec A, Kramberger C, Georgakilas V, Prato M, Kuzmany H. A detailed Raman study on thin single-wall carbon nanotubes prepared by the HiPCO process. *Eur Phys J B* 2002;28(2):223–30.
- [14] Yudasaka M, Kataura H, Ichihashi T, Qin LC, Kar S, Iijima S. Diameter enlargement of HiPco single-wall carbon nanotubes by heat treatment. *Nano Lett* 2001;1(9):487–9.
- [15] Zhou W, Ooi YH, Russo R, Papanek P, Luzzi DE, Fischer JE, et al. Structural characterization and diameter-dependent oxidative stability of single wall carbon nanotubes synthesized by the catalytic decomposition of CO. *Chem Phys Lett* 2001;350(1–2):6–14.
- [16] Zoican Loebick C, Abanulo D, Majewska M, Haller GL, Pfefferle LD. Effect of reaction temperature in the selective synthesis of single wall carbon nanotubes (SWNT) on a bimetallic CoCr-MCM-41 catalyst. *Appl Catal A* 2010;374(1–2):213–20.
- [17] Mudimela PR, Nasibulin AG, Jiang H, Susi T, Chassaing D, Kauppinen EI. Incremental variation in the number of carbon nanotube walls with growth temperature. *J Phys Chem C* 2009;113(6):2212–8.
- [18] Su Y, Yang Z, Wei H, Kong ES-W, Zhang Y. Synthesis of single-walled carbon nanotubes with selective diameter distributions using DC arc discharge under CO mixed atmosphere. *Appl Surf Sci* 2011;257(7):3123–7.
- [19] Kataura H, Kumazawa Y, Maniwa Y, Ohtsuka Y, Sen R, Suzuki S, et al. Diameter control of single-walled carbon nanotubes. *Carbon* 2000;38(11–12):1691–7.
- [20] Nasibulin AG, Pikhitsa PV, Jiang H, Kauppinen EI. Correlation between catalyst particle and singlewalled carbon nanotube diameters. *Carbon* 2005;43(11):2251–7.
- [21] Husnu Emrah U, Manish C. Investigation of single-walled carbon nanotube growth parameters using alcohol catalytic chemical vapour deposition. *Nanotechnology* 2005;16(10):2153–63.
- [22] Yao Y, Li Q, Zhang J, Liu R, Jiao L, Zhu YT, et al. Temperature-mediated growth of single-walled carbon-nanotube intramolecular junctions. *Nat Mater* 2007;6(4):283–6.
- [23] Picher M, Anglaret E, Arenal R, Jourdain V. Processes controlling the diameter distribution of single-walled carbon nanotubes during catalytic chemical vapor deposition. *ACS Nano* 2011;5(3):2118–25.
- [24] Saito T. Efficient and controlled synthesis of SWCNTs by enhanced direct injection pyrolytic synthesis (eDIPS) method and their applications, Guadalupe workshop The Fifth Rice University, Air Force Research Laboratory, and NASA workshop on nucleation and growth mechanisms of single wall carbon nanotubes, Texas, USA; 8–12 April, 2011. p. 79. http://swcntnanoriceedu/uploadedFiles/SWCNT_Workshop/024_Saito.pdf.
- [25] Moaisala A, Nasibulin AG, Brown DP, Jiang H, Khriachtchev L, Kauppinen EI. Single-walled carbon nanotube synthesis using ferrocene and iron pentacarbonyl in a laminar flow reactor. *Chem Eng Sci* 2006;61(13):4393–402.
- [26] Kivisto S, Hakulinen T, Kaskela A, Aitchison B, Brown DP, Nasibulin AG, et al. Carbon nanotube films for ultrafast broadband technology. *Opt Express* 2009;17(4):2358–63.
- [27] Sun DM, Timmermans MY, Nasibulin AG, Kauppinen EI, Kishimoto S, Mizutani T, et al. High-performance carbon nanotube thin-film transistors and logic circuits on flexible substrate. *Nat Nanotechnol* 2011;6(3):156–61.
- [28] Kaskela A, Nasibulin AG, Zavodchikova MY, Aitchison B, Papadimitratos A, Tian Y, et al. Aerosol synthesized SWCNT networks with tuneable conductivity and transparency by dry transfer technique. *Nano Lett* 2010;10(11):4349–55.
- [29] Nasibulin AG, Kaskela A, Mustonen K, Anisimov AS, Ruiz V, Kivisto S, et al. Multifunctional free-standing single-walled carbon nanotube films. *ACS Nano* 2011;5(4):3214–21.
- [30] Moaisala A, Nasibulin AG, Shandakov SD, Jiang H, Kauppinen EI. On-line detection of single-walled carbon nanotube formation during aerosol synthesis methods. *Carbon* 2005;43(10):2066–74.
- [31] Bhowmick R, Clemens BM, Cruden BA. Parametric analysis of chirality families and diameter distributions in singlewall carbon nanotube production by the floating catalyst method. *Carbon* 2008;46(6):907–22.
- [32] Tian Y, Jiang H, Pfaler JV, Zhu Z, Nasibulin AG, Nikitin T, et al. Analysis of the size distribution of single-walled carbon nanotubes using optical absorption spectroscopy. *J Phys Chem Lett* 2010;1(7):1143–8.
- [33] Hofmann S, Sharma R, Ducati C, Du G, Mattevi C, Cepek C, et al. In situ observations of catalyst dynamics during surface-bound carbon nanotube nucleation. *Nano Lett* 2007;7(3):602–8.
- [34] Lolli G, Zhang L, Balzano L, Sakulchaicharoen N, Tan Y, Resasco DE, et al. Tailoring (n,m) structure of single-walled carbon nanotubes by modifying reaction conditions and the nature of the support of CoMo catalysts. *J Phys Chem B* 2006;110(5):2108–15.
- [35] Anisimov AS, Nasibulin AG, Jiang H, Launois P, Cambedouzo J, Shandakov SD, et al. Mechanistic investigations of single-walled carbon nanotube synthesis by ferrocene vapor decomposition in carbon monoxide. *Carbon* 2010;48(2):380–8.
- [36] Nasibulin AG, Brown DP, Queipo P, Gonzalez D, Jiang H, Kauppinen EI. An essential role of CO₂ and H₂O during single-walled CNT synthesis from carbon monoxide. *Chem Phys Lett* 2006;417(1–3):179–84.